Impact Resistance of Potential Replacement Materials for Large Power Transformer Tanks

Jide Williams , Joseph Hoffman * , Paul Predecki * , Maciej Kumosa *

Posted Date: 12 November 2024

doi: 10.20944/preprints202408.0513.v2

Keywords: Ballistic Impact; Large Power Transformers; Numerical Simulations; Steel and Composite Plates; Polyurea

Article

Potential Impact Protection of Polymer Matrix Composite Panels using Polyurea Coatings

Jide Williams [1,*], Joseph Hoffman [2] Paul Predecki [2] and Maciej Kumosa [2]

[1] Walter Scott, Jr. College of Engineering, Scott, Bioengineering Building, 700 Meridian Ave, Fort Collins, CO 80523

[2] Center for Novel High Voltage/Temperature Materials and Structures, University of Denver, 2155 E Wesley Ave, Denver, CO 80208

* Correspondence: jide.williams@colostate.edu

Abstract: The protective effect of polymer coatings on Polymer Matrix Composite (PMC) panels against high-velocity ballistic impacts specifically as a potential replacement material for Large Power Transformer Tanks (LPT) has not been widely investigated. In particular, numerical predictions of the ballistic performance of the panels with coatings under impact are not available which is not surprising considering the complexity of the problem due to the prohibitive cost of the experimental testing. This numerical study was performed to understand the potential beneficial effects of a polyurea (PU) coating on PMCs, in application in LPT tanks. Glass fiber/epoxy and carbon fiber/epoxy composite panels individually and in a hybrid combination were subjected to 400 m/s ballistic impact. Using finite elements, the impact damage evolution for uncoated panels was investigated to determine the arrest depth as a function of panel thickness. Subsequently, the panels were evaluated for their ballistic response in the presence of PU coatings. It has been shown numerically for the first time that the addition of PU was three times more efficient in protecting the glass and carbon fiber panels against penetration than by increasing their thickness. In all three cases, adding a coating of PU decreased the estimated cost, mass, and thickness of the panels required to prevent penetration of the modeled projectile.

Keywords: Index Terms—Ballistic Impact; Polymer Matrix Composite Plates; Polyurea; Numerical Simulations

1. Introduction

Polymer matrix composites (PMCs) are being used for structural and ballistic protection applications. This numerical study of the capabilities of PMCs to withstand ballistic impact came about as a follow-up to a research proposal to utilize PMCs as the structural materials in large power transformer (LPT) tanks [1]. LPTs are a key component of the electrical grid, and their reliability is critical for health, safety, and economic prosperity. However, in the last ten years, certain LPTs have been the target of vandalism. Aside from the rifle attack on the Metcalf substation in California on April 16, 2013 [2] which caused roughly $16 million in damage, an analysis done by the Wall Street Journal reported that there were 274 cases of power grid vandalism in the United States between 2012 and 2014 [3,4]. The authors of [1] suggested that PMCs can favorably mitigate impact damage and other challenges as the reliability of grid components becomes critical in the presence of increasing vandalism. The current study aims to model hybrid combinations of two common PMCs with and without a Polyurea (PU) coating to identify potential structures that could minimize cost and weight, two very significant factors in many materials selection decisions. Results of our ballistic simulations of PMCs with and without an extra coating of protective Polyurea (PU) presented in this work could apply to any PMC plates utilized for structural or protective purposes.

PMCs for ballistic impact protection have been widely studied both experimentally and numerically. Authors of [5], provided a comprehensive review of various PMCs and the factors that influence their reaction to impacts including material, geometry, environment, and projectile type and velocity. The authors of [6], using a continuum damage mechanics model, modeled the effects of projectile size and velocity for a carbon fiber/epoxy panel. The authors of [7] both modeled and

 doi:10.20944/preprints202408.0513.v2

conducted experimental impact tests on Carbon Fiber Reinforced Polymer (CFRP) panels for both non-woven and woven architectures. In [8], ballistic impact tests of Glass Fiber Reinforced Polymer (GFRP) composites were conducted. In this study they found that the ballistic performance could be improved by adding expensive nanoparticles to the epoxy matrix. For the purpose of verifying our model, we utilized a less recent study by Kasano [9] in which he experimentally tested the ballistic limit and residual velocities for CFRP plates as a function of the impact velocity.

Hybrid structures have also been evaluated. In experimental work done by [10,11], the authors proposed a PMC laminate sandwich architecture consisting of two different composite types that offered the best impact resistance over several other composite architectures with an improvement of over 40 times. The laminate consisted of face sheets of 5 unidirectional CFRP plies (top and bottom) with a core made up of 10 plies of unidirectional GFRP. The improved impact resistance of the sandwich structure was attributed to the process of delamination at the CFRP/GFRP interfaces which was shown to absorb much of the energy. However, the investigation was limited to quasi-static loads.

PU's ballistic resistance capability is known to be due to its so-called 'high-strain rate sensitivity'. Under high strain rates (10^5/s to 10^7/s) [12,13], certain types of PU respond with high shear strength which can be higher than that of steel. The shear strength of PU in a ballistic event greatly depends on the thickness of the substrate [13]. In a high pressure and strain rate situation, PU's shear strength can exceed most engineering materials that are used in protection technology. When used as a coating on metals and composites an impact resistant polymer should have a significant glass transition temperature well below LPT operating temperatures which could be -20 to about 300 °C. It has been shown in [14] and discussed by [12], that for PU the strain-rate-induced glass transition (the broad α-transition) leads to enhanced energy dissipation upon impact. This occurs when the deformation rate is comparable to the rate of motion of the soft segment in the PU chain, which for several PUs is of the order of 10^5 to 10^7/s at room temperature. At quasi-static strain rates (10^{-2}/s) this α-transition occurs around -50 to -60 °C, well below LPT operating temperatures. For the LPT tank, PU could offer significant additional advantages in terms of durability and resilience for protection against environmental elements. PU has an estimated 75-year life span [15], with good resistance to ultraviolet (UV) light.

PU has been used as a coating for several substrates such as steel, aluminum, ceramics, etc. [13], [15–19] but has only been recently studied as a coating for brittle composites such as CFRP to improve blast resistance [20]. A very interesting observation made in [20] was that placing the PU on the rear side of the CFRP textile structure provided significantly better spalling protection than having the coating on the front side. Zhang et al [21], have provided a comprehensive review of PU and its use in blast and impact protection for various substrates. For ballistic protection, the authors indicated that PU is generally placed on the front of the substrates, and this is more feasible in LPT tanks as it avoids PU contact with the transformer fluid. The authors also identified certain disadvantages such as the difficulty in repairing damaged coatings, spraying and coating problems due to uneven mixing, and the elevated costs of its preparation and application, which can greatly influence its effectiveness when used as coating for protection. In a related study on the impact behavior of porcelain bushings on LPTs, it was shown that the bushings can be protected against impact when coated with Polyurethane-Urea (LINEX) [22–24]. With the advent of big data and machine learning, convolutional neural networks (CNN) have been used to predict the dynamic cohesive properties (DCPs) of a bicontinuosly nanostructured copolymer such as PU [25]

In this work, Finite Element (FE) Analysis was used to analyze the ballistic impact resistance of PMC materials (see Figure 1). To accomplish this, versatile FE models were built using Python scripts for use with the Abaqus Explicit solver, utilizing various material models. For the verification of the FE model, the work done by [9] and [26] was utilized where a carbon fiber cross-ply PMC plate served as the target.

Once the validations were completed, simulations were conducted using CFRP and GFRP to determine minimum thicknesses required to prevent ballistic penetration of a 400 m/s 12.7 mm spherical steel projectile. In addition, the effect of composite hybridization was evaluated using

 doi:10.20944/preprints202408.0513.v2

laminates with half CFRP and half GFRP. Finally, the significant benefit of adding a thin PU coating to the underlying substrates was analyzed numerically. While as noted there have been experiments conducted to evaluate the ballistic protection benefits of adding a PU coating to PMCs, we believe this is the first flexible numerical simulation to be conducted.

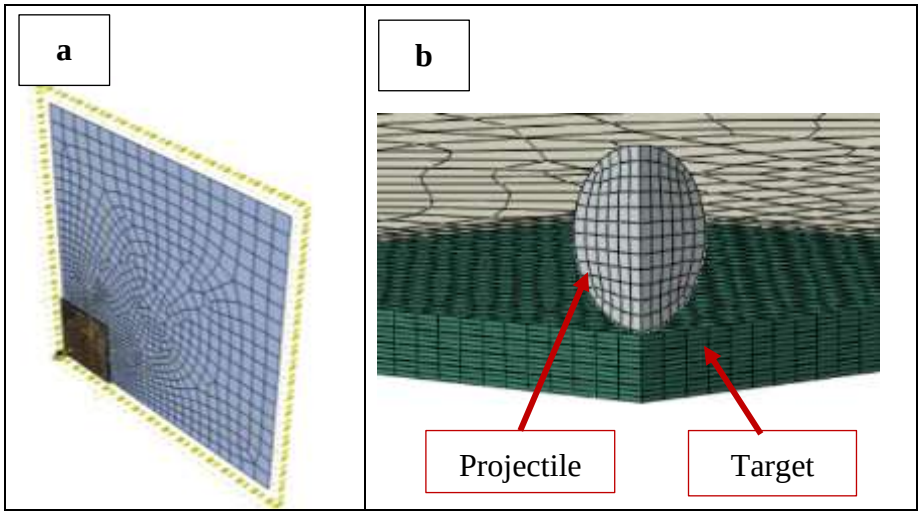

Figure 1. Numerical model of a composite plate under impact: (a) plate and target and (b) relative dimensions of target and projectile.

2. Materials and Failure Models

Failure models describing the onset and evolution of failure used in our numerical simulations were a "User Subroutine" in ABAQUS [27] developed by Dassault Systems for the PMCs, the Prony series and a Virtual User Defined Field (VUSDFLD) for PU [28,29], and the Johnson-Cook model (JC) [28] for the projectile. The script developed allows for the joint application of diverse material models when analyzing several different impact conditions.

A cross-ply CFRP epoxy laminate and a cross-ply GFRP epoxy laminate were analyzed individually, and in combination as a hybrid composite. The properties of the CFRP laminae came from [26]. The properties of GFRP were computed using Helius Composite software and its references and knowledge network [30]. The properties for these materials are displayed in Table 1.

Table 1. CFRP and GFRP Unidirectional (UD) Laminae Properties.

Description	CFRP [26]	GFRP [30]
Young's modulus, E_{11} (GPa)	235	53
Young's modulus, E_{22} (GPa)	17	12.4
Young's modulus, E_{33} (GPa)	17	12.4
Poisson's ratio n_{12}	0.32	0.26
Poisson's ratio n_{13}	0.32	0.26
Poisson's ratio n_{23}	0.45	0.45
Shear modulus, G_{12} (GPa)	4.5	4.18
Shear modulus, G_{13} (GPa)	4.5	4.18

 doi:10.20944/preprints202408.0513.v2

Shear modulus, G_{23} (GPa)	2.5	4.27
Tensile Failure Stress, X_{1t} (MPa)	3900	2750
Comp. Failure Stress, X_{1c} (MPa)	2400	1470
Tensile Failure Stress, X_{2t} (MPa)	111	59.6
Comp. Failure Stress, X_{2c} (MPa)	290	293
Tensile Failure Stress, X_{3t} (MPa)	50	59.6
Comp. Failure Stress, X_{3c} (MPa)	290	293
Failure Shear Stress, S_{12} (MPa)	120	122.6
Failure Shear Stress, S_{13} (MPa)	137	124
Failure Shear Stress, S_{23} (MPa)	90	124

The user subroutine for composite progressive damage, was made available by Simulia [26] in their documentation. The material properties of CFRP linked to the user subroutine that was applied in this study were also from [26] and are summarized in Table 1. The user subroutine was enhanced by utilizing Hashin's damage model for composites [31] for the initiation and evolution of the through-thickness damage to the fiber and matrix for PMCs. In the subroutine, the Hashin damage criterion was specified for the fiber failure mode while the Puck criterion [26,32] was applied to the matrix damage modes. The relationship between fiber and matrix damage utilized in the user subroutine is given by [26]:

$$\text{Fiber damage (tension): } d = \left(\frac{\sigma_{11}}{X_{1tf}}\right)^2 + \left(\frac{\tau_{12}}{S_{12f}}\right)^2 + \left(\frac{\tau_{13}}{S_{13f}}\right)^2 \quad (1)$$

$$\text{Fiber damage (compression): } d = \frac{|\sigma_{11}|}{X_{1cf}} \quad (2)$$

Matrix tension and compression (Puck)

$$d = \left[\left(\frac{\sigma_{11}}{2X_{1tm}}\right)^2 + \frac{\sigma_{22}^2}{X_{2tm}.X_{2cm}} + \left(\frac{\tau_{12}}{S_{12m}}\right)^2\right] + \sigma_{22}\left(\frac{1}{X_{2tm}} + \frac{1}{X_{2cm}}\right) \quad (3)$$

Where $\sigma_{ij}, and\ \tau_{ij}$, are the effective stress tensors, $X_{1tf}, X_{1cf}, S_{12f}$, and S_{13f} are the fiber tensile, compressive, and shear strengths. X_{1tm}, and X_{2tm}, are the matrix tensile failure stress in the 1 and 2 directions (1 is the fiber direction), X_{2cm} is the matrix compressive failure stress in the 2-direction, and S_{12m}, is the matrix failure shear stress.

For PU, a single composition was chosen to demonstrate the effectiveness of PU coatings in attenuating impact on the PMC panels. The particular PU composition ratio, namely 4-parts by weight of Versalink P-1000 diamine to 1-part of Isonate 143L isocyanate, was selected for two reasons. Firstly, this composition has been extensively studied by research groups funded by the US Office of Naval Research at UCLA and UCSD, , with the 4:1 ratio being generally considered optimal for impact applications [33]. Secondly, a Prony series for the viscoelastic response of this PU composition was available [29]. This composition ratio is close to being stoichiometric since the equivalent weights are 575-625 g/equivalent for the Versalink P-1000 [34], and 144.5 g/equivalent for the Isonate 143L [35] resulting in a mass ratio of 3.98-4.35:1 for a stoichiometric ratio of 1:1 for the amine to isocyanate groups.

The material properties of the particular PU investigated by [29] are listed in Table 2. PU exhibits a linear and viscous response in its stress/strain characteristics. The time-dependent behavior of PU is attributed to the material's hard and soft segments, i.e., the motion of the chain at different time scales. PU has been modeled as a linear viscoelastic isotropic solid material by [29] using the material's shear relaxation modulus G. The Prony series was used in [21] and in this work to model

 doi:10.20944/preprints202408.0513.v2

the relaxation of a polymer consisting of *n* decaying exponentials. Equations 4 and 5 describe the time dependent shear and bulk moduli of PU under high strain rates [36].

$$G_t = \left[G_\infty + \sum_{k=1}^{n} g_k G_0 . \exp\left(-\frac{t}{\tau_k}\right)\right] \text{ where } g_k = \frac{G_k}{G_0} \quad (4)$$

$$K_t = \left[K_\infty + \sum_{k=1}^{n} k_k K_0 . \exp\left(-\frac{t}{\tau_k}\right)\right] \text{ where } k_k = \frac{K_k}{K_0} \quad (5)$$

The terms g_k and k_k in equations (4) and (5) are the ratios of the shear and bulk moduli to the shear and bulk moduli of the kth element at the onset of deformation, and τ_k is the relaxation time of the kth element, that is the time it takes to 'relax' the stress to about 38% (1/*e*) of the initial applied stress. G_0, and K_0 are the shear and bulk moduli at time t = 0, G_∞, K_∞ are the shear and bulk moduli of the first element in the generalized Maxwell model. These are the viscous properties needed for input in a Prony series in the time domain in the Abaqus explicit simulation. In this work, 14 terms of the Prony series, provided by the experimental work of [29] were used in the simulation.

Finally, a Virtual User Defined Field (VUSDFLD) [28] subroutine was used to assess the response of PU. VUSDFLD is a custom constitutive model used for modeling the high strain rate behavior of PU. The VUSDFLD subroutine computes the strain in the material at each time step using the Prony series and then compares it with a critical strain value at which the material fails. With limited published data on critical strain values for PU at the strain rates under study, we selected a failure value of 0.25 to perform element elimination from the model. We believe this value of 0.25 is conservative given stress-strain curves for various PUs that we reviewed [13,37,38].

Table 2. Material Properties for Polyurea [29] at room temperature.

Density (kg/m^3)		1071
Elastic Modulus (GPa)		1.084
Bulk Modulus (GPa)		4.54
Poisson's Ratio		0.486
Viscous Properties (Prony Series) [29]		
g_k	k_k	τ_k (s)
0.03691	0.03691	1.00E-13
0.03691	0.03691	5.00E-13
0.03691	0.03691	1.00E-12
4.10E-17	4.10E-17	1.00E-11
0.222841	0.222841	1.00E-10
0.176243	0.176243	1.00E-09
0.116726	0.116726	1.00E-08
0.092643	0.092643	1.00E-07
0.063106	0.063106	1.00E-06
0.042889	0.042889	1.00E-05
0.037371	0.037371	0.0001
0.019091	0.019091	0.001
0.016129	0.016129	0.01
0.010039	0.010039	0.1

For the projectile, the material model and the calibrated Johnson-Cook (J-C) failure parameters as shown in Table 3 were used. The material response is linear elastic up to its yield strength, after

 doi:10.20944/preprints202408.0513.v2

which it deforms plastically until its failure strain [28]. The yield stress ($\bar{\sigma}_Y$) and the strain at failure ($\bar{\varepsilon}_f$) [39] are expressed by equations (6) and (7).

$$\bar{\sigma}_Y(A,B,n,C,\dot{\bar{\varepsilon}}_0,T_m,T_0,m) = \left[A + B\left(\bar{\varepsilon}_{pl}\right)^n\right]\left[1 + C\, ln\frac{\dot{\bar{\varepsilon}}_{pl}}{\dot{\bar{\varepsilon}}_0}\right]\left[1 - \left(\frac{T-T_0}{T_m-T_0}\right)^m\right] \quad (6)$$

$$\bar{\varepsilon}_f(d_1,d_2,d_3,d_4,d_5,\dot{\bar{\varepsilon}}_0,\ T_m,T_0) = \left[d_1 + d_2\exp\left(d_3\eta\right)\right]\left[1 + d_4\ln\left(\frac{\dot{\bar{\varepsilon}}_{pl}}{\dot{\bar{\varepsilon}}_0}\right)\right]\left(1 + d_5\frac{T-T_0}{T_m-T_0}\right) \quad (7)$$

In equations 6 and 7, η= -p⁄q represents the triaxiality, defined as the hydrostatic pressure divided by the deviatoric stress or (Von Mises stress), $\dot{\bar{\varepsilon}}_0$ is the reference strain rate, T is the attained temperature of the material, T_m is the melting point, T_0 is the ambient temperature or the reference temperature, $\bar{\varepsilon}_{pl}$ is the plastic strain, and $\dot{\bar{\varepsilon}}_{pl}$ the plastic strain rate, C is the viscous effect constant, n is the strain hardening exponent, m is the thermal softening exponent, and $d_1, d_2, d_3, d_4,$ and d_5 are damage parameters.

Table 3. Johnson-Cook properties for 4340 steel projectiles.

Description	Notation	4340 Steel [40]
Modulus of elasticity	E (GPa)	208
Poisson's ratio	ν	0.3
Density	$\rho\left({}^{kg}/_{m^3}\right)$	7830
Yield Stress	$A\ (MPa)$	792
Strain hardening constant and exponent	$B\ (MPa)$ n	510 0.26
Viscous effect	C	0.014
Thermal softening constant	m	1.03
Reference strain rate	$\dot{\bar{\varepsilon}}_0$	0.000333
Melting temperature	$T_m\ (K)$	1700
Transition temperature	$T_0\ (K)$	571

During impact, the high plastic strain rate causes the dissipation of energy as heat which raises the temperature (T) of each of the impacted elements in the model. The temperature rise is exclusive to each element and there is no heat conduction assumed between the elements. The inelastic heat

 doi:10.20944/preprints202408.0513.v2

fraction applied in the simulation was 0.9, that is, 90% of the energy dissipated by the plastic deformation was converted to heat.

3. Independent Verification of FE Models

To confirm the validity of the PMC model, a comparison was made to an experiment conducted by [9]. In that work, a 5 mm diameter spherical steel projectile of mass 0.51 g was fired at three different velocities at a multi-ply composite panel and the residual velocities were measured. The composite panel was a $[0,90,0]_{ns}$ laminate with 12 or 18 layers of CFRP, in which n=2 or 3 respectively, and the panel thickness ranged from 1.8 mm to 2.7 mm. For this validation, the 12-layer (n=2) experiment was used. A PMC 200 x 200 mm panel was simulated with a target area of 50 x 50 mm to reduce computation costs. Taking advantage of symmetry, a quarter model was developed as seen in Figure 1a and b. The architecture, plies, and thickness of the model followed those of the experiment [9]. The target was divided into sub-laminates, where each [0,90,0] sub-laminate was separated by a cohesive zone. The cohesive zones were modeled with cohesive elements (COH3D8) with maximum degradation set to 1 kJ.

The finite element model is shown in Figure 1. The region of the plate outside the target area was modeled with shell elements (S4R) to reduce the computational cost. The target region was represented with first-order C3D8R continuum elements [26] (layer-by-layer) to capture the damage in detail. Edges of the plate were fixed in place. To make the model more versatile, a python script was used to develop the model where geometry conditions, mesh parameters, contact parameters, speed of the projectile, and boundary conditions were defined as variables.

The exact properties of the steel projectile used in the experiment in [9] were not stated. In our work cold- rolled steel was used to model the projectile as a deformable spherical solid following [26]. We specifically selected cold-rolled 4340 steel for the projectile. The projectile yield followed the Johnson-Cook parameters listed in Table 3. These complete parameters may be used to simulate both the initiation and propagation of the damage in the projectile under elastoplastic conditions. However, this study limits the projectile to a perfectly elastic material in order to simplify the model.

A mesh sensitivity study was conducted for the target with mesh sizes of between 0.3 and 1.0 mm, and for the projectile, with mesh sizes of between 0.35mm and 0.55mm. A good correlation was found with the experimental result at mesh sizes of 0.85 mm in the planar directions and at one element per ply in the thickness direction (0.15 mm) for the target and 0.4 mm for the projectile. We utilized the tools developed by [24] but compared our simulation results directly with the experiment [23] due to some concerns about the geometry assumptions used by [24].

Preprints.org (www.preprints.org) | NOT PEER-REVIEWED | Posted: 12 November 2024 doi:10.20944/preprints202408.0513.v2

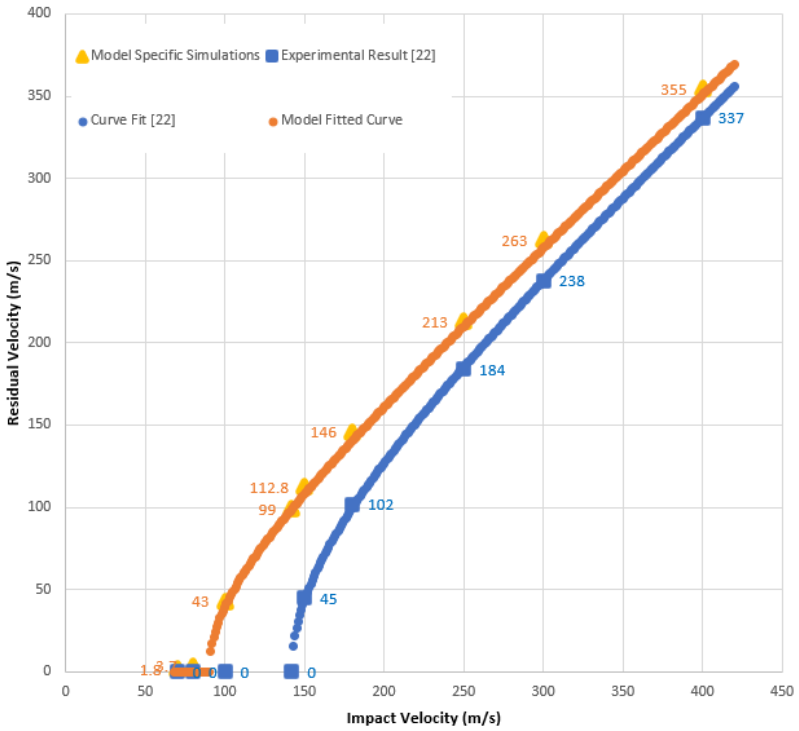

Figure 2. Comparison of CFRP model with experimental results from [9].

The bottom curve in Figure 2 is the fitted curve from [9] for the 12-layer panel. This fitted curve utilizes the function:

$$V_R = \alpha\sqrt{V_i^2 - V_{bl}^2} \quad (8)$$

where V_i is the impact velocity, V_{bl} is the ballistic limit, and α is a function of the mass of the projectile and the masses of the fragments released from the plate upon impact (for more information see [9]). Certain points along that curve are specified for comparison with the model where those same velocities were simulated. A curve using the same parameters as the experiment (i.e., with α = 0.9) is fitted to those points and displayed in the top curve of Figure 2. It is to be noted that while the variation in the residual velocities decreases as impact velocity increases as shown in Figure 2, the difference in the residual kinetic energies of the projectile between the experiment and the simulation stays roughly constant. Using either measure, the simulation produces a conservative estimate of the energy dissipated by the composite plates and thus the actual results should be better than those predicted by the modeling.

4. Impact Response of CFRP and GFRP Plates

Next, the impact resistance of CFRP and GFRP composites was evaluated using the same model that was verified in the previous section. All of the simulations utilized individual unidirectional 0.2 mm plies in a [0/90/0] architecture. Thus each [0/90/0] sub-laminate was 0.6 mm thick. The target and plate lateral dimension were the same as those used in the PMC verification. Again, C3D8R elements were used in the target area and S4R elements in the non-target area. Lateral dimensions of 0.85 mm and thickness dimensions of 0.2 mm were used for the PMC target element mesh sizes. The thickness dimension of the PMC mesh corresponded to one element per ply. The edges of the plates were likewise fixed.

 doi:10.20944/preprints202408.0513.v2

At first 18 layers of sub-laminates for a total thickness of 10.8 mm for both CFRP and GFRP were found in the simulation to be penetrated by a 400 m/s 4340 steel spherical projectile with a 5 mm diameter. The PMC thickness is similar to the standard thickness of an LPT tank [1] . The thicknesses for both the CFRP and the GFRP plates were then increased by adding additional sub-laminates to find the minimum thickness that would prevent penetration. Subsequently, a consistent thickness of 27.6 mm was evaluated to allow for the comparison of penetration depths and to see whether penetration depths would significantly change if the thicknesses were increased beyond the minimum penetration prevention thickness. See Figure 3 a and b for simulation schematics. The results are presented in Table 4(a).

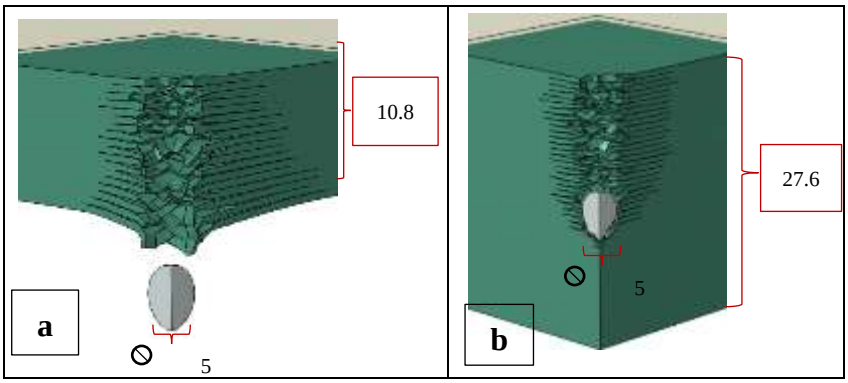

Figure 3. Penetrations of and arrests in CFRP plates using a 400 m/s projectile: **(a)** penetration in 10.8 mm plate and **(b)** arrest in a 27.6 mm thick plate.

Following the proposal of [10], two hybrid architectures of CFRP/GFRP and GFRP/CFRP (where the projectile impacts the first material listed before the second and both components were of equal thickness) were evaluated. In both cases, the initial 10.8 mm thick hybrid plates were unable to prevent full penetration from the 400 m/s steel projectile. The same process to estimate minimum thicknesses and penetration depths as discussed in the prior paragraph was then conducted for these hybrid structures. The results are presented in Table 4(b).

The results in Table 4 show that the projectiles were arrested with a 19.8 mm thick CFRP plate and a 21.2 mm GFRP plate. When the thicknesses for both of these structures were increased to 27.6 mm, the arrest distances were similar to those for the near minimum arrest thickness plates. The results in table 4a clearly show that there are critical arrest distances for the projectile at 400 m/s which are between 17.1 and 17.3 for CFRP and between 21.2 and 20.8 for GFRP. It can also be seen that when the thickness was increased by approximately 30-40%, the critical arrest distances did not change materially. This suggests that we can simulate the projectile arrest with plate thickness relatively close to the arrest distance. However, this might create a bulge at the backface of the plate containing delaminations which could affect the projectile arrest process. The projectile would be stopped but the backface would be severely damaged leading to a partial arrest. Consistent results were obtained using hybrid CFRP + GFRP plates, regardless of their order (Table 6b). However, the significant improvements from hybridization as reported by [10] and [11] were not observed in our simulations.

Table 4. Penetration results from 400 m/s test with 4340 steel projectiles: a) CFRP and GFRP laminates, b) CFRP and GFRP hybrid composites.

Target (Individual PMCs) **a**	Structure Thickness (mm)	Arrest Depth I (mm)	Constant Structure thickness (mm)	Arrest Depth II (mm)
CFRP	19.8	17.1	27.6	17.3
GFRP	22.2	21.2	27.6	20.8

 doi:10.20944/preprints202408.0513.v2

Target (Hybrid PMCs) b	Structure Thickness (mm)	Arrest Depth I (mm)	Constant Structure thickness (mm)	Arrest Depth II (mm)
CFRP + GFRP	19.8	17.6	27.6	17.5
GFRP + CFRP	21.6	18.7	27.6	18.8

5. The Effect of PU Coating

The modeling of the PMCs with PU utilized the same PMC mesh sizes and a mesh size of 0.3 mm for the PU. With the addition of 3 mm of PU to the original 10.8 mm thick plates, the CFRP/PU plate successfully arrested the 400 m/s projectile as shown in Table 5. Figure 4 illustrates the simulated results. However, with the GFRP plate, the addition of the PU only allowed for the partial arrest of the projectile. A hybrid combination of PU/CFRP/GFRP with a total thickness of 13.8 mm also successfully arrested the projectile. Table 7 in comparison with Table 5 reveals the significant effect of the 3 mm PU coating on CFRP and GFRP plates having 10.8 mm thicknesses.

For the CFRP and the hybrid CFRP-GFRP plates with the PU coating, the 400 m/s projectile was fully arrested. However, the coated GFRP allowed partial penetration. In this case, the thickness of the coating or of the GFRP would have to be increased in order to achieve a full arrest, but likely nowhere near the approximately 20 mm thickness required without the coating. Thus, by applying a 3 mm coating of PU, the thickness of the CFRP composite plate to just prevent penetration could be significantly reduced.

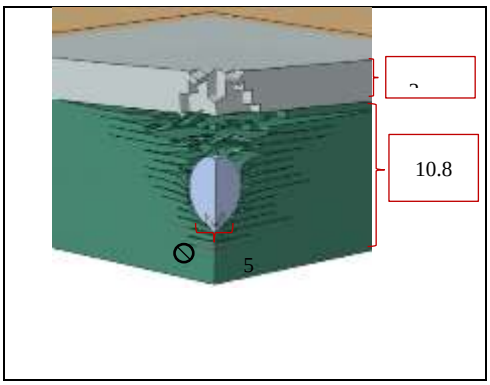

Figure 4. Penetration of and arrest in a 10.8 mm CFRP plate coated with 3 mm of PU using a 400 m/s projectile.

These results show that PU could play a major role in the impact protection of advanced PMCs, for example in the protection of LPT tanks. To further demonstrate this effect, Figures 5 and 6 are presented. We analyzed the damage formation process in the PU/CFRP/GFRP laminate (fig. 5), from the onset of the projectile impact until the projectile is fully arrested inside the laminate. Eight stages of the damage progression between 0 to150 microseconds are shown. Figure 6 shows the velocities of the projectile in the hybrid laminate with and without the PU coating.

Table 5. Penetration results from 400 m/s test with 4340 steel projectiles: CFRP, GFRP, and hybrid composites with PU coating.

Target (individual PMCs with coating)	Structure Thickness (mm)	Arrest Depth Depth (mm)
3 mm PU + 10.8 mm CFRP	13.8	12.05

 doi:10.20944/preprints202408.0513.v2

3 mm PU + 10.8 mm GFRP	13.8	13.77 (partial penetration)
3 mm PU + 5.4 mm CFRP + 5.4 mm GFRP	13.8	12

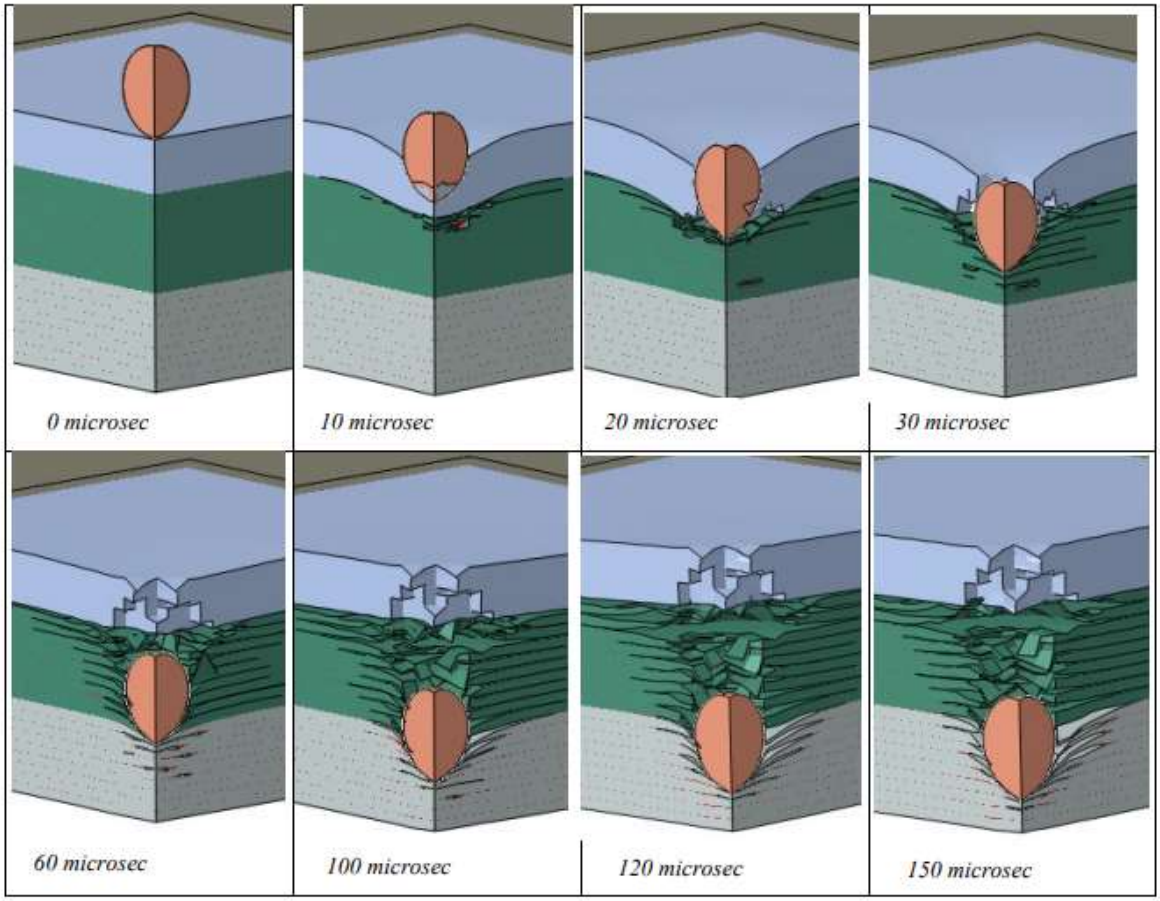

Figure 5. Progressive penetration of the projectile through the coated hybrid.

Several important observations can be made when analyzing the data presented in figs. 5 and 6. First, the projectile decelerations (change in velocities) are markedly different between the coated and uncoated composites in Figure 6. The reduction in the velocity of the projectile in the coating is significantly larger than in the composite. For example, the time it takes for the projectile to decelerate from 400 to 200 m/s with PU is approximately 15 microseconds while for the same deceleration without PU it takes about 45 microseconds which is 3 times longer. Thus the PU has a significantly beneficial effect on the deceleration of the projectile. At somewhere between 10 and 20 microseconds the projectile has just penetrated the PU coating (Fig. 5). Note that while the coated plates fully arrested the projectile and brought its velocity to zero, the projectile retained an exit velocity of about 200 m/s after penetrating the uncoated hybrid laminate.

 doi:10.20944/preprints202408.0513.v2

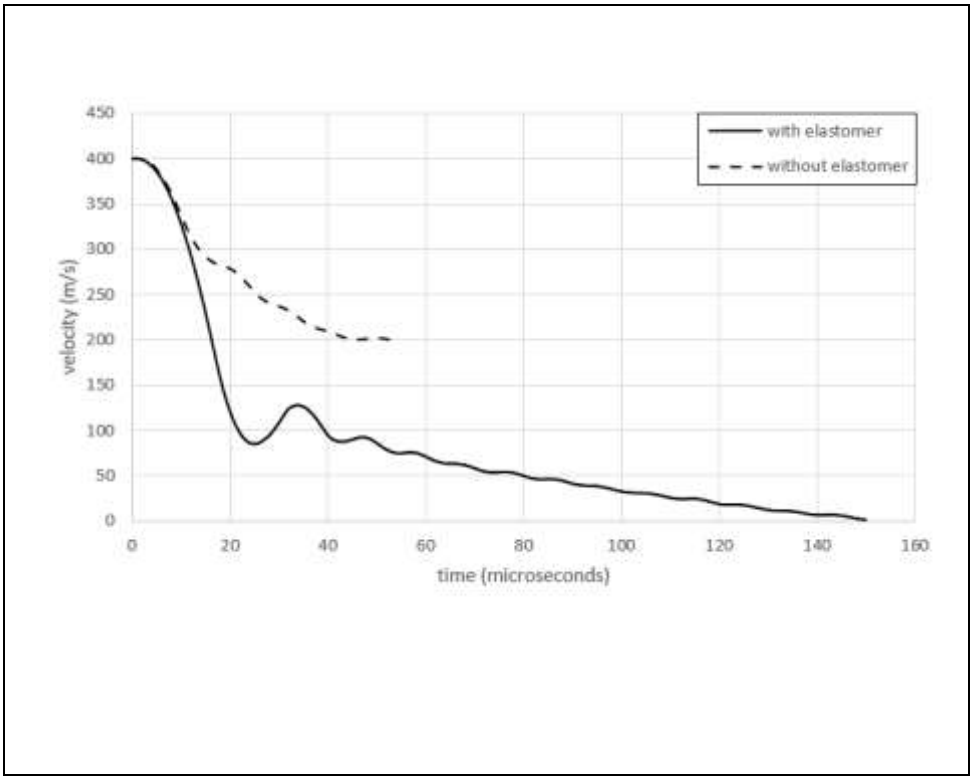

Figure 6. Velocities versus time after impact for the hybrid with and without 3mm elastomer coating.

Using estimated costs of $25, $5, and $22.50 /kg and densities of 1750, 1870, and 1071 kg/m^3 for CFRP, GFRP, and PU respectively, along with the simulated results from Tables 4 and 5, Table 6 summarizes the modeled thicknesses to pervent penetration for all six material combinations studied. It also estimates the costs and masses of the material options. It is clear from this table that adding a 3 mm coating of PU reduces the thickness, cost, and mass required to prevent penetration for any of the substrate materials.

Table 6. Thickness, cost, and mass of material combinations required to prevent ballistic penetration: CFRP, GFRP, and hybrid composites with and without PU coating.

Material	Required Thickness (mm)	Cost / Square Meter	Mass (kg)/ Square Meter (kg)
CFRP	19.8	$866.25	34.7
GFRP	22.8	$213.18	42.6
CFRP+GFRP	19.8	$525.69	35.8
PU+CFRP	13.8	$544.79	22.1
PU+GFRP	13.8*	$173.27	23.4
PU+CFRP+GFRP	13.8	$359.03	22.8

*Partial penetration

 doi:10.20944/preprints202408.0513.v2

7. Conclusions

This research analyzed CFRP, GFRP, and CFRP/GFRP plates either uncoated or coated with Polyurea under projectile impact at 400m/s. This was done by performing dynamic FE simulations using a steel projectile. Using our independently verified FE models, we determined that the perforation of the plates and the arrest of the projectile all strongly depend on the type of materials simulated and their thicknesses.

Simulated CFRP, GFRP, and CFRP/GFRP composite plates behave in a very similar fashion under 4340 steel projectile impact. The damage evolution in the composites was essentially the same with the arrest depths ranging from 17 to 21 mm. When the thicknesses of the plates were increased by about 30-40 %, the depths of arrest did not significantly change.

PU was seen to significantly improve the simulated ballistic response of the PMC plates. When a 3 mm PU coating was applied to a 10.8 mm CFRP plate, the steel projectile was arrested at about 12 mm depth. Meanwhile, there was a partial penetration for GFRP of the same thickness and coating. The CFRP/GFRP hybrid with coating showed a similar arrest depth as that of the CFRP with coating. We showed that the projectile decelerated from 400 to 200 m/s in 15 microseconds for the PU/CFRP/GFRP sample while it took three times longer to reach that same reduced velocity in the 10.8 mm uncoated hybrid sample.

While the value of PU coatings on PMCs has previously been shown experimentally and numerically for other purposes as mentioned in the introduction, in our research, we have evaluated the required thickness of PU to be applied to the standard LPT tank thickness to prevent ballistic penetration for a specified projectile. Based on our numerical predictions, PU could be more efficient at improving ballistic resistance than simply increasing the base material thickness.

Based on our validation, our models underestimate the energies absorbed by the composites. We believe this indicates that actual composite plates could perform even better than what the simulations have shown. Therefore, for projectile impacts up to at least 400 m/s, a CFRP/GFRP composite could potentially be a good material for LPT tanks when PU coatings are applied.

Depending on the design and material requirements for the substrate, a different selection of materials could be made. For example, if the structural needs could be met by GFRP, Table 6 would indicate that GFRP with a PU coating is the cheapest option to provide ballistic protection. On the other hand, if cost is not a consideration, PU + CFRP is the lightest option. PU + CFRP + GFRP may be a good compromise between cost and mass. For each of the three underlying substrates, adding PU instead of increasing thickness reduced both cost and weight. These results come from testing 10.8 mm thick substrates with 400 m/s impacts so further analysis would be required for other base thicknesses and velocities. Of course, before being used in any real-life applications, our simulation results would need to be verified experimentally. The cost of potential experimental verification is presently beyond available financial resources of the authors. However, the number of costly experiments could be significantly reduced by application of these simulation results. Therefore, the models and the simulation results presented in this work could be quite valuable in the design of the actual experimental impact testing on the selected composite panels for application in LPT tanks.

ACKNOWLEDGMENTS: This work was supported by the US Department of Energy and other members of the National Science Foundation (NSF) Industry/University Cooperative Research Center for Novel High Voltage/Temperature Materials and Structures (HVT Center) under Grant IIP 1362135.

References

1. J. Williams, J. Hoffman, P. Predecki, and M. S. Kumosa, "Application of Polymer Matrix Composites in Large Power Transformer Tanks," *IEEE Transactions on Power Delivery*, pp. 1–1, 2022, doi: 10.1109/TPWRD.2022.3147410.
2. Siemens, "Bullet resistant power transformer retrofit." Siemens Industry, Inc, 2018.
3. R. Smith, "Assault on California Power Station Raises Alarm on Potential for Terrorism," WSJ. Accessed: Dec. 05, 2022. [Online]. Available: http://online.wsj.com/article/SB10001424052702304851104579359141941621778.html

4. Mike Sheppard, Saqib Saeed, "Bullet and weather concerns driver of retrofits in US market," Bullet and weather concerns driver of retrofits in US market. [Online]. Available: https://powertechresearch.com/bullet-and-weather-concerns-driver-of-retrofits-in-us-market/
5. J. J. Andrew, S. M. Srinivasan, A. Arockiarajan, and H. N. Dhakal, "Parameters influencing the impact response of fiber-reinforced polymer matrix composite materials: A critical review," *Composite Structures*, vol. 224, p. 111007, Sep. 2019, doi: 10.1016/j.compstruct.2019.111007.
6. D. Long, "Simulation of ballistic impact on polymer matrix composite panels," *Journal of Theoretical and Applied Mechanics*, no. Vol. 53 nr 2, pp. 263–272, 2015, doi: 10.15632/jtam-pl.53.2.263.
7. S. Chocron, A. J. Carpenter, N. L. Scott, R. P. Bigger, and K. Warren, "Impact on carbon fiber composite: Ballistic tests, material tests, and computer simulations," *International Journal of Impact Engineering*, vol. 131, pp. 39–56, Sep. 2019, doi: 10.1016/j.ijimpeng.2019.05.002.
8. N. Domun *et al.*, "Ballistic impact behaviour of glass fibre reinforced polymer composite with 1D/2D nanomodified epoxy matrices," *Composites Part B: Engineering*, vol. 167, pp. 497–506, Jun. 2019, doi: 10.1016/j.compositesb.2019.03.024.
9. H. Kasano, "Impact perforation of orthotropic and quasi-isotropic CFRP laminates by a steel ball projectile," *Advanced Composite Materials*, vol. 10, no. 4, pp. 309–318, Jan. 2001, doi: 10.1163/156855101753415337.
10. P. Beaumont, P. Riewald, and C. Zweben, "Methods for Improving the Impact Resistance of Composite Materials," in *Foreign Object Impact Damage to Composites*, L. Greszczuk, Ed., 100 Barr Harbor Drive, PO Box C700, West Conshohocken, PA 19428-2959: ASTM International, 1975, pp. 134-134–25. doi: 10.1520/STP33154S.
11. B. Lusk, "Blast Protection for Power Transformer - Blast and Ballistic Final Report," *National Institute for Hometown Security (NIHS)-University of Kentucky*, 2012.
12. Y. Sun, S. E. Kooi, K. A. Nelson, A. J. Hsieh, and D. Veysset, "Impact-induced glass-to-rubber transition of polyurea under high-velocity temperature-controlled microparticle impact," *Appl. Phys. Lett.*, vol. 117, no. 2, p. 021905, Jul. 2020, doi: 10.1063/5.0013081.
13. R. G. S. Barsoum, Elastomeric Polymers with High Rate Sensitivity: Applications in Blast, Shockwave, and Penetration Mechanics. William Andrew, 2015.
14. R. B. Bogoslovov, C. M. Roland, and R. M. Gamache, "Impact-induced glass transition in elastomeric coatings," *Appl. Phys. Lett.*, vol. 90, no. 22, p. 221910, May 2007, doi: 10.1063/1.2745212.
15. Primeaux Associates LLC, "Polyurea Technology Life Expectancy Discussion".
16. Y. Jiang, B. Zhang, J. Wei, and W. Wang, "Study on the impact resistance of polyurea-steel composite plates to low velocity impact," *International Journal of Impact Engineering*, vol. 133, p. 103357, Nov. 2019, doi: 10.1016/j.ijimpeng.2019.103357.
17. D. T., A. Gobiraman, P. Venkatachalam, M. Anish, J. Jayaprabakar, and J. Sajin, "Effect of Plural Spray Coating Process Parameters on Bonding Strength of Polyurea with Steel and Aluminum for Liquid Storage Applications," Jun. 2020, doi: 10.1520/JTE20200061.
18. Y. Xiao, Z. Tang, and X. Hong, "Low velocity impact resistance of ceramic/polyurea composite plates: experimental study," *J Mech Sci Technol*, vol. 35, no. 12, pp. 5425–5434, Dec. 2021, doi: 10.1007/s12206-021-1113-z.
19. H. Kim, J. Citron, G. Youssef, A. Navarro, and V. Gupta, "Dynamic fracture energy of polyurea-bonded steel/E-glass composite joints," *Mechanics of Materials*, vol. 45, pp. 10–19, Feb. 2012, doi: 10.1016/j.mechmat.2011.08.017.
20. Q. Liu *et al.*, "Investigating ballistic resistance of CFRP/polyurea composite plates subjected to ballistic impact," *Thin-Walled Structures*, vol. 166, p. 108111, Sep. 2021, doi: 10.1016/j.tws.2021.108111.
21. R. Zhang, W. Huang, P. Lyu, S. Yan, X. Wang, and J. Ju, "Polyurea for Blast and Impact Protection: A Review," *Polymers*, vol. 14, no. 13, Art. no. 13, Jan. 2022, doi: 10.3390/polym14132670.
22. C. N. Henderson, C. S. DeFrance, P. Predecki, and M. Kumosa, "Damage prevention in transformer bushings subjected to high-velocity impact," *International Journal of Impact Engineering*, vol. 130, pp. 1–10, Aug. 2019, doi: 10.1016/j.ijimpeng.2019.03.007.
23. C. N. Henderson, J. Monteith, E. Solis-Ramos, R. Godard, P. Predecki, and M. Kumosa, "Impact protection of borosilicate glass plates with elastomeric coatings in drop tower tests," *International Journal of Impact Engineering*, vol. 137, p. 103460, Mar. 2020, doi: 10.1016/j.ijimpeng.2019.103460.
24. C. N. Henderson *et al.*, "Ballistic fragmentation confinement of coated brittle transformer bushing models," *International Journal of Impact Engineering*, vol. 122, pp. 363–373, Dec. 2018, doi: 10.1016/j.ijimpeng.2018.08.017.
25. H. Jin, T. Jiao, R. J. Clifton, and K.-S. Kim, "Dynamic fracture of a bicontinuously nanostructured copolymer: A deep-learning analysis of *big-data-generating experiment*," *Journal of the Mechanics and Physics of Solids*, vol. 164, p. 104898, Jul. 2022, doi: 10.1016/j.jmps.2022.104898.
26. Simulia, "Projectile Impact on a Carbon Fiber Reinforced Plate," Apr. 2007.
27. Smith, Michael, *ABAQUS/Standard User's Manual, Version 6.9*. Dassault Systèmes Simulia Corp.

28. Abaqus v 6.6 Documentaion, "ABAQUS User Reference Manual." [Online]. Available: https://classes.engineering.wustl.edu/2009/spring/mase5513/abaqus/docs/v6.6/books/sub/default.htm?startat=ch01s02asb04.html
29. C. A. Gamez, "Failure mechanisms of polyurea under high strain-rate," UCLA, 2017. Accessed: Feb. 06, 2022. [Online]. Available: https://escholarship.org/uc/item/10c9c1qq
30. "References | Helius Composite | Autodesk Knowledge Network." Accessed: Oct. 20, 2022. [Online]. Available: https://knowledge.autodesk.com/support/helius-composite/learn-explore/caas/CloudHelp/cloudhelp/2017/ENU/ACMPDS/files/GUID-062281EC-35AD-4201-AB7B-D43282175B22-htm.html
31. "Failure Criteria for Unidirectional Fiber Composites | J. Appl. Mech. | ASME Digital Collection." Accessed: Jan. 27, 2022. [Online]. Available: https://asmedigitalcollection.asme.org/appliedmechanics/article-abstract/47/2/329/390775/Failure-Criteria-for-Unidirectional-Fiber?redirectedFrom=PDF
32. "References | Helius PFA 2016 | Autodesk Knowledge Network." Accessed: Jan. 27, 2022. [Online]. Available: https://knowledge.autodesk.com/support/helius-pfa/learn-explore/caas/CloudHelp/cloudhelp/2016/ENU/ACMPAN/files/GUID-2F40E192-7868-4AA7-8820-DE7CCE7C2B6C-htm.html
33. G. Vijay, "Visco Elastic Models," Sep. 14, 2024.
34. "Coatings & Adhesives Journal 2023." Accessed: Oct. 01, 2024. [Online]. Available: http://coatings-and-adhesives-journal.evonik.com/index.php
35. T. D. C. Company, "ISONATE™ 143L Modified MDI".
36. Ever J. Barbero, *Finite Element Analysis of Composite Materials Using Abaqus*. Boca Raton, FL 33487-2742: CRC Press, 2013.
37. R. G. Rinaldi, M. C. Boyce, S. J. Weigand, D. J. Londono, M. W. Guise, "Microstructure evolution during tensile loading histories of a polyurea," *Wiley Online Library*, vol. 49, no. 23, pp. 1660–1671, Sep. 2011, doi: https://doi.org/10.1002/polb.22352.
38. Yuexin Jiang, Boyi Zhang , Jianshu Wei, Wei Wang, "Study on the dynamic response of polyurea coated steel tank subjected to blast loadings," *Science direct*, vol. 67, Sep. 2020, doi: https://doi.org/10.1016/j.jlp.2020.104234.
39. "Abaqus Analysis User's Guide (2016)." Accessed: Nov. 01, 2022. [Online]. Available: http://130.149.89.49:2080/v2016/books/usb/default.htm?startat=pt05ch23s02abm23.html#d0e265842
40. B. Banerjee, "Material point method simulations of fragmenting cylinders," Jan. 2012.